Plexin D1 determines body fat distribution by regulating the type V collagen microenvironment in visceral adipose tissue

James E. N. Minchin[a,b], Ingrid Dahlman[c], Christopher J. Harvey[b], Niklas Mejhert[c], Manvendra K. Singh[d,e], Jonathan A. Epstein[d], Peter Arner[c], Jesús Torres-Vázquez[f], and John F. Rawls[a,b,1]

[a]Department of Molecular Genetics and Microbiology, Duke University, Durham, NC 27710; [b]Department of Cell Biology and Physiology, University of North Carolina at Chapel Hill, Chapel Hill, NC 27599; [c]Department of Medicine, Karolinska Institutet, Karolinska University Hospital, 14186 Stockholm, Sweden; [d]Cell and Developmental Biology and the Cardiovascular Institute, University of Pennsylvania, Philadelphia, PA 19104; [e]Signature Research Program in Cardiovascular and Metabolic Disorders, Duke-National University of Singapore Graduate Medical School, National Heart Center, 169857 Singapore; and [f]Department of Cell Biology, Helen L. and Martin S. Kimmel Center for Biology and Medicine at the Skirball Institute, New York University School of Medicine, New York, NY 10016

Edited* by Roger D. Cone, Vanderbilt University School of Medicine, Nashville, TN, and approved February 11, 2015 (received for review August 27, 2014)

Genome-wide association studies have implicated *PLEXIN D1* (*PLXND1*) in body fat distribution and type 2 diabetes. However, a role for *PLXND1* in regional adiposity and insulin resistance is unknown. Here we use in vivo imaging and genetic analysis in zebrafish to show that Plxnd1 regulates body fat distribution and insulin sensitivity. Plxnd1 deficiency in zebrafish induced hyperplastic morphology in visceral adipose tissue (VAT) and reduced lipid storage. In contrast, subcutaneous adipose tissue (SAT) growth and morphology were unaffected, resulting in altered body fat distribution and a reduced VAT:SAT ratio in zebrafish. A VAT-specific role for Plxnd1 appeared conserved in humans, as *PLXND1* mRNA was positively associated with hypertrophic morphology in VAT, but not SAT. In zebrafish *plxnd1* mutants, the effect on VAT morphology and body fat distribution was dependent on induction of the extracellular matrix protein collagen type V alpha 1 (*col5a1*). Furthermore, after high-fat feeding, zebrafish *plxnd1* mutant VAT was resistant to expansion, and excess lipid was disproportionately deposited in SAT, leading to an even greater exacerbation of altered body fat distribution. Plxnd1-deficient zebrafish were protected from high-fat-diet-induced insulin resistance, and human VAT *PLXND1* mRNA was positively associated with type 2 diabetes, suggesting a conserved role for *PLXND1* in insulin sensitivity. Together, our findings identify Plxnd1 as a novel regulator of VAT growth, body fat distribution, and insulin sensitivity in both zebrafish and humans.

zebrafish | body fat distribution | adipose development | insulin resistance | extracellular matrix

The regional distribution and morphology of adipose tissue (AT) are strong predictors of metabolic disease (1–3). Excess lipid deposition in visceral AT (VAT; adipose associated with visceral organs) is associated with increased susceptibility to insulin resistance and type 2 diabetes (4), whereas expansion of subcutaneous AT (SAT; adipose between muscle and skin) is associated with reduced risk for metabolic disease and is even protective against hyperglycemia and dyslipidemia (4–7). In turn, hypertrophic AT morphology (few large adipocytes) is associated with insulin resistance and AT dysfunction, whereas hyperplastic AT morphology (many small adipocytes) is associated with improved metabolic parameters (4, 7–9). Therefore, the identification of factors that regulate regional distribution and AT morphology could lead to new therapies to treat metabolic disease.

Genome-wide association studies have implicated the *PLEXIN D1* (*PLXND1*) locus in waist:hip ratio (a measurement of regional AT distribution) and type 2 diabetes (10). However, a role for Plxnd1 in AT morphology, distribution, and metabolism is unknown. Plxnd1 is a transmembrane receptor that controls the migration, proliferation, and survival of diverse cell types (11). Mutation of Plxnd1 in mouse and zebrafish leads to hypervascularization in many tissues (12, 13), and vascular endothelial cell Plxnd1 modulates extracellular matrix (ECM) synthesis and composition by regulating the collagen receptor, β1-integrin (14). In turn, ECM provides a supportive microenvironment for AT growth and function (15). For example, type V collagens regulate collagen fiber assembly, geometry, and strength (16, 17), are up-regulated during adipogenesis, and can stimulate adipocyte differentiation in vitro (18–20). However, the role of type V collagens during in vivo AT growth is unknown.

In this study, we use genetic analysis and in vivo imaging of lipid deposition dynamics in zebrafish to assess the role of Plxnd1 in AT morphology and body fat distribution. Previous studies have shown that zebrafish adipocytes and AT are morphologically, molecularly, and functionally homologous to mammalian white AT (21–26), and like mammals, zebrafish adipocytes accumulate a large cytoplasmic lipid droplet (LD) that facilitates the in vivo identification of adipocytes by fluorescent lipophilic dyes (21, 22, 24–26). Here we determine in zebrafish that Plxnd1 functions through Col5a1 to exert a VAT-specific effect on adipose growth and morphology, resulting in altered body fat distribution and improved insulin sensitivity. In accord, molecular and physiological assessments in

Significance

***PLEXIN D1* (*PLXND1*) has been implicated in body fat distribution and type 2 diabetes by genome-wide association studies, but the mechanism is unknown. We show here that Plxnd1 regulates body fat distribution in zebrafish by controlling the visceral adipose tissue (VAT) growth mechanism. Plxnd1 deficiency in zebrafish resulted in induction of a hyperplastic state and reduced lipid deposition in VAT. Regulation of VAT was dependent on the induction of the type V collagen, *col5a1*, suggesting that Plxnd1 controls body fat distribution by determining the status of VAT extracellular matrix. Plxnd1-deficient zebrafish were protected from high-fat-induced insulin resistance, and human *PLXND1* mRNA was positively associated with type 2 diabetes. These results suggest that the role of Plxnd1 in body fat distribution and insulin signaling is conserved from zebrafish to humans.**

Author contributions: J.E.N.M., I.D., N.M., J.A.E., P.A., and J.F.R. designed research; J.E.N.M., I.D., C.J.H., N.M., and P.A. performed research; J.E.N.M., I.D., C.J.H., N.M., M.K.S., and P.A. analyzed data; J.E.N.M., I.D., M.K.S., J.T.-V., and J.F.R. wrote the paper.

The authors declare no conflict of interest.

*This Direct Submission article had a prearranged editor.

[1]To whom correspondence should be addressed. Email: john.rawls@duke.edu.

This article contains supporting information online at www.pnas.org/lookup/suppl/doi:10.1073/pnas.1416412112/-/DCSupplemental.

humans support a conserved role for *PLXND1* in regulation of VAT morphology and insulin sensitivity.

Results

Zebrafish *plxnd1* Mutants Have Reduced Lipid Accumulation in VAT and Altered Body Fat Distribution. To test the role of Plxnd1 in body fat distribution, we first analyzed lipid deposition in homozygous Plxnd1 knockout mice; however, these mice die at birth before extensive formation of VAT (*SI Appendix*, Fig. S1). Therefore, we turned to the zebrafish model system. Homozygous *plxnd1* null zebrafish mutants and their phenotypically normal siblings were stained with the neutral lipid dye Nile Red, and individual ATs were categorized into VAT, SAT or miscellaneous AT (cranial or associated with the skeleton) (Fig. 1*A* and *SI Appendix*, Fig. S2*A*). We then measured AT area, which has been previously shown to accurately predict triacylglyceride content (24). Total AT area per fish was indistinguishable between *plxnd1* mutants and siblings (Fig. 1 *A* and *B* and *SI Appendix*, Fig. S2*B*), and total extracted lipid levels per fish were identical (*SI Appendix*, Fig. S2*C*). However, VAT area and volume were significantly decreased in *plxnd1* mutants (Fig. 1 *A* and *B* and *SI Appendix*, Fig. S2*D*). In contrast, no significant change was observed between *plxnd1* mutants and siblings in SAT or miscellaneous AT-localized lipid storage (Fig. 1*B* and *SI Appendix*, Fig. S2*D*), suggesting Plxnd1 exerts a VAT-specific effect. The decrease in VAT area in *plxnd1* mutants led to a reduced VAT:SAT ratio (Fig. 1*B*). Thus, mutation of *plxnd1* in zebrafish is associated with reduced lipid storage in VAT and altered body fat distribution.

***Plxnd1* Deficiency Induces a Hyperproliferative and Hyperplastic State in Zebrafish VAT.** We next quantified LD number and size as measures of hyperplastic and hypertrophic AT morphology (25). Both sibling and *plxnd1* mutant VAT had a bimodal distribution of LD sizes containing a population of very small LDs that was unaltered between genotypes (Fig. 1 *C* and *D*), as well as a second population of large LDs that was significantly smaller in *plxnd1* mutants compared with in siblings (Fig. 1 *C* and *D* and *SI Appendix*, Fig. S3*A*). Volumetric measurements supported the smaller size of *plxnd1* mutant VAT LDs (*SI Appendix*, Fig. S3 *B* and *C*). Furthermore, *plxnd1* mutants had a greater number of LDs per unit volume (Fig. 1*C* and *SI Appendix*, Fig. S3*D*), and histology confirmed the hyperplastic morphology of *plxnd1* mutant VAT (*SI Appendix*, Fig. S3 *E–G*). *plxnd1* mutant VAT had a greater number of 5-ethynyl-2-deoxyuridine–labeled (EdU^+) proliferating cells than sibling VAT (Fig. 1 *C* and *E*), of which the majority of EdU^+ nuclei belonged to either adipocytes or endothelial cells (Fig. 1*F* and *SI Appendix*, Fig. S4). Further, quantitative RT-PCR (qRT-PCR) revealed an increased expression of adipocyte differentiation genes (Fig. 1*G*). In contrast, the morphology of *plxnd1* SAT was indistinguishable from that of siblings (*SI Appendix*, Fig. S5). Together, these data demonstrate that Plxnd1 deficiency induces adipocyte hyperproliferation, induction of adipocyte differentiation genes, and hyperplastic VAT morphology without affecting SAT morphology.

***PLXND1* mRNA Is Positively Associated with Hypertrophic Morphology in Human VAT, but not SAT.** As Plxnd1 deficiency in zebrafish led to VAT-specific changes in morphology and altered body fat distribution, we next investigated whether a similar relationship existed in humans. Multiple regression analysis (adjusting for age and body mass index) revealed a positive association between VAT *PLXND1* mRNA and more pronounced hypertrophic morphology in VAT ($R^2 = 0.22$ and $P = 0.031$) (Fig. 1*H*), although no correlation was observed between *PLXND1* mRNA and morphology in SAT (*SI Appendix*, Fig. S2*E*). Thus, these data demonstrate that *PLXND1* mRNA exhibits a VAT-specific association with morphology in humans, wherein greater levels of *PLXND1* mRNA are associated with VAT hypertrophy and lower levels of *PLXND1* mRNA are associated with hyperplastic VAT morphology. These data, together with the zebrafish data, suggest a conserved role for Plxnd1 in promoting hypertrophic VAT morphology.

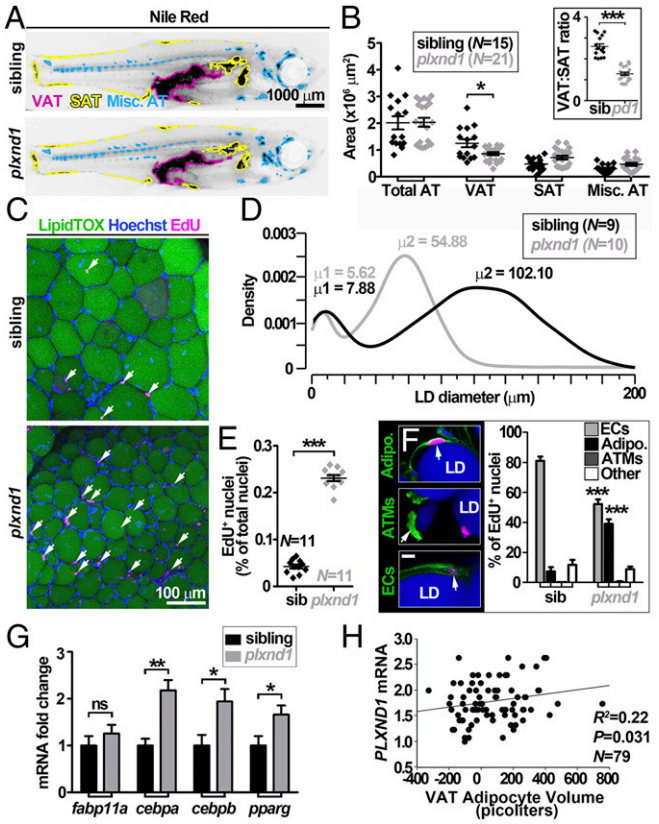

Fig. 1. Reduced VAT volume and hyperplastic morphology underlie an altered body fat distribution in *plxnd1* mutant zebrafish. (*A*) Fluorescent stereoscope images of Nile Red-stained zebrafish inverted and false colored according to VAT (magenta), SAT (yellow), or miscellaneous AT (blue). Fish were 10.1 mm standard length. (*B*) VAT area is reduced in *plxnd1* zebrafish ($P = 0.0115$), leading to a decreased VAT:SAT ratio (inset, $P < 0.0001$). There were trends toward increases in SAT ($P = 0.142$), miscellaneous AT ($P = 0.053$), and total adiposity ($P = 0.085$) that did not reach statistical significance ($\alpha = 0.05$). (*C*) Maximum-intensity projections of zebrafish VAT stained with LipidTOX (LDs, green), Hoechst (nuclei, blue), and EdU (proliferative nuclei, magenta). Arrows indicate EdU^+ nuclei. (*D*) Probability density functions to represent VAT-LD diameter distributions. VAT-LD diameters were modeled using a mixture of two normal distributions. The mean (μ) of each distribution is indicated (μ1 and μ2). (*E*) Quantification of EdU+ nuclei normalized to total nuclei from Z-stacks. (*F*) Colocalization of EdU+ nuclei (magenta) with LD-containing adipocytes (Adipo.), as identified using the plasma membrane dye CellMask (green) and LipidTOX (blue); AT macrophages (ATMs), as identified by WCL15 antibody reactivity (green); and endothelial cells (ECs), as identified by EGFP (green), from the *fli1a:EGFP* transgenic line. Quantification of EdU+ nuclei in these cell types revealed a significant increase in endothelial cells and adipocytes in *plxnd1* mutants. (*G*) The mRNA levels for adipocyte differentiation markers *cebpa, cebpb*, and *pparg* were increased in *plxnd1* VAT by qRT-PCR. *Fabp11a*, a homolog of mammalian *Fabp4/aP2*, was unchanged. (*H*) A significant positive correlation was observed between VAT *PLXND1* mRNA and hypertrophic VAT morphology in humans. No correlation was observed in human SAT (*SI Appendix*, Fig. S2*E*). Fish were ~12 mm standard length unless otherwise stated.

Col5a1 Is Induced by Vascular Endothelial Cells of *plxnd1* Mutant VAT. Because Plxnd1 is known to modulate ECM synthesis and composition (14, 27), we next analyzed ECM dynamics in *plxnd1* mutant zebrafish. qRT-PCR revealed large-scale dysregulation of ECM components within *plxnd1* mutant VAT (Fig. 2*A*). In general, ECM components were down-regulated (Fig. 2*A*);

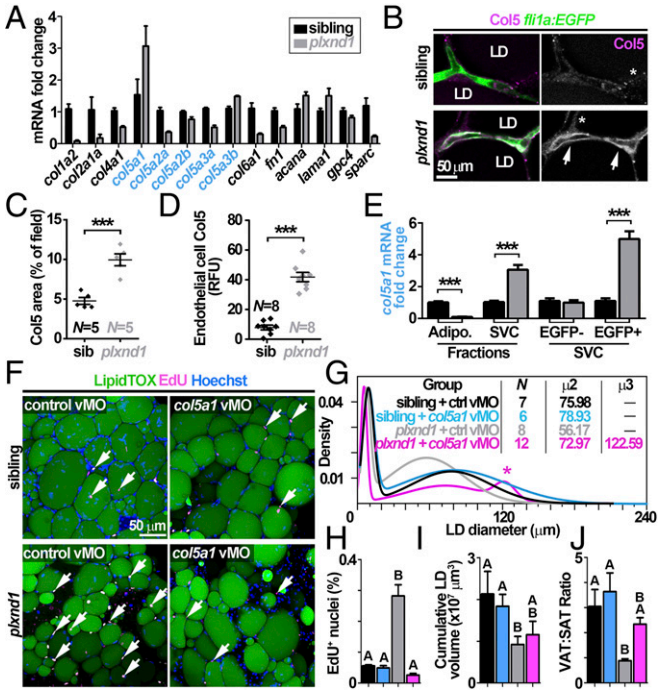

Fig. 2. Col5a1 is essential for maintenance of the hyperproliferative and hyperplastic state of *plxnd1* mutant VAT. (*A*) qRT-PCR for ECM markers from whole zebrafish VAT reveals an up-regulation of *col5a1* in *plxnd1* VAT. All mRNAs shown were significantly different between *plxnd1* and siblings ($\alpha = 0.05$). (*B*) Immunofluorescence for type V collagens (Col5) (*Left*, magenta; *Right*, white) reveals increased Col5 accumulation in association with endothelial cells in *plxnd1* VAT (arrows). Asterisks indicate nonendothelial peri-adipocyte localized Col5. (*C*) Quantification of Col5 area. Area is expressed as percentage of field of view. (*D*) Quantification of Col5 signal in endothelial cells relative to background. (*E*) qRT-PCR on adipocyte (Adipo.) and SVC fractions reveals *col5a1* is enriched in SVCs of *plxnd1* VAT. FACS enrichment of EGFP+ endothelial cells from *fli1a:EGFP plxnd1* mutant and sibling VAT show that SVC-derived *col5a1* is up-regulated in *plxnd1* endothelial cells. (*F*) Maximum-intensity projections of VAT from sibling or *plxnd1* animals injected with either control or *col5a1* vMO. Images are from i1e2-injected animals; however, results were identical with both vMOs. Fish were ~9 mm standard length. (*G*) Probability density functions to represent VAT-LD diameter distributions after manipulation of *col5a1*. VAT-LD diameters were modeled using a mixture of two or three normal distributions. The mean (μ) of each distribution is indicated (μ1, μ2, and μ3). (*H*) Injection of *col5a1* vMO normalizes the hyperproliferation observed in *plxnd1* VAT. (*I*) Injection of *col5a1* vMO increases VAT cumulative volume in *plxnd1* mutants. (*J*) Injection of *col5a1* vMO increases the VAT:SAT ratio in *plxnd1* mutants. For *F–J*, data were pooled from both *col5a1-i1e2* and *col5a1-e3i3* vMO-injected animals.

however, the type V collagens *col5a1* and *col5a3b* were increased (Fig. 2*A*). Intriguingly, type V collagens have been previously shown to induce proliferation and differentiation of preadipocytes in vitro (19, 20) and regulate collagen fibrillogenesis to control ECM geometry and tensile strength (16, 17), properties that have been implicated in metabolic dysfunction of obese AT (28). Immunofluorescence confirmed an increase in Col5 protein and revealed specific localization to vascular endothelial cells in *plxnd1* mutant VAT (Fig. 2 *B–D* and *SI Appendix*, Fig. S6), a site previously associated with COL5A1 protein localization in human AT (18). FACS enrichment of endothelial cells followed by qRT-PCR determined that *col5a1* mRNA was increased in *plxnd1* mutant endothelial cells (Fig. 2*E*), supporting a vascular endothelial cell origin for Col5a1 in *plxnd1* mutant VAT.

Knockdown of Col5a1 Normalizes Hyperproliferation and Hyperplastic Morphology Within *plxnd1* Mutant VAT. We hypothesized that induction of Col5a1 in *plxnd1* mutant VAT establishes a microenvironment conducive to hyperplastic growth. To test this, we targeted zebrafish *col5a1* with multiple, nonoverlapping vivo-morpholinos (vMOs). Serial injection of either vMO disrupted splicing of *col5a1*, and RT-PCR followed by sequencing confirmed the production of truncated *col5a1* mRNAs predicted to be nonfunctional (*col5a1-i1e2*, 55 amino acids; *col5a1-e3i3*, 112 amino acids) (*SI Appendix*, Fig. S7 *C* and *D*). Assessment of Col5 reactivity after injection of *col5a1-i1e2* vMO revealed significantly reduced Col5 protein levels in both endothelial cell and periadipocyte locations (*SI Appendix*, Fig. S8). Injection of either *col5a1* vMO did not affect proliferation or morphology of sibling VAT (Fig. 2 *F–H*). However, in hyperplastic *plxnd1* mutant VAT, injection of *col5a1* vMO increased LD hypertrophy and induced the appearance of an additional population of very large LDs (μ3 = 122.59 μm; Fig. 2 *F* and *G*). Further, *col5a1* vMO normalized levels of EdU^+ nuclei in *plxnd1* mutant VAT (Fig. 2 *F* and *H*), and volumetric analysis revealed a partial rescue of lipid storage in *plxnd1* mutant VAT (Fig. 2*I*), thus increasing the VAT:SAT ratio (Fig. 2*J*). Therefore, Col5a1 is required for maintenance of the hyperplastic state of *plxnd1* mutant VAT and the resulting body fat distribution.

***plxnd1* Mutant VAT Undergoes Augmented Fibrillogenesis in a Col5a1-Dependent Manner.** Our data suggest that zebrafish Plxnd1 modulates body fat distribution by determining the status of the VAT ECM microenvironment. To ascertain the architectural properties of ECM, we used the fluorescent collagen probe 5-(4,6-dichlorotriazinyl) aminofluorescein to label VAT-localized collagen fibers (*SI Appendix*, Fig. S9*A*) (28). ECM architecture of *plxnd1* mutant VAT was markedly different from that of sibling VAT (Fig. 3*A*) and was characterized by larger and more numerous interstitial collagen fibers (Figs. 3*A* and *SI Appendix*, Fig. S10). Moreover, *plxnd1* mutant VAT had increased glycoprotein, elastin content (*SI Appendix*, Fig. S11), and a greater abundance of fibrous ECM (*SI Appendix*, Fig. S11). *plxnd1* mutant SAT did not have altered collagen or fibrous ECM (*SI Appendix*, Fig. S11 *H* and *I*), again demonstrating the starkly different response of VAT and SAT to Plxnd1 deficiency. To assess fibrillogenesis in *plxnd1* mutant VAT, we extracted ECM from zebrafish VAT and induced polymerization and gel formation in vitro (*SI Appendix*, Fig. S12). We then conducted turbidity assays to determine the rate and ultimate extent of fibrillogenesis. Plxnd1-deficient VAT underwent an increased rate of fibrillogenesis compared with sibling ECM (Fig. 3*B*), and *plxnd1* mutant VAT attained a higher ultimate turbidity than sibling VAT (Fig. 3*C*). Injection of *col5a1-i1e2* vMO did not affect in vitro fibrillogenesis of sibling VAT; however, *col5a1* vMO injection significantly reduced both the rate of fibrillogenesis and ultimate turbidity in *plxnd1* mutant VAT (Fig. 3 *B* and *C*). Therefore, ECM from *plxnd1* mutant VAT has markedly different properties than wild-type VAT and undergoes augmented fibrillogenesis in a Col5a1-dependent manner.

***plxnd1* Mutant ECM Is Sufficient to Induce Hyperproliferation and Hyperplastic Morphology of Stromal Vascular Cells In Vitro.** We next wished to test whether ECM of Plxnd1-deficient VAT is sufficient to instruct VAT cell proliferation and morphology. Isolated ECM from zebrafish VAT was used as a substrate for the culture of primary stromal vascular cells (SVCs) also isolated from zebrafish VAT (Fig. 3*D*). When cultured within a 3D ECM substrate obtained from sibling VAT, sibling SVCs were able to proliferate and readily differentiate into adipocytes containing large LDs (Fig. 3 *E* and *G*). In contrast, *plxnd1* mutant SVCs cultured on ECM derived from *plxnd1* mutant ECM reached a higher level of confluency (Fig. 3 *E* and *F* and *SI Appendix*, Fig. S13*A*), together with strikingly smaller LDs (Fig. 3 *E* and *G* and *SI Appendix*, Fig. S13*A*). The degree of confluency and LD hypertrophy were ECM extract-dependent, as culturing sibling SVCs within ECM from *plxnd1* mutants increased confluency and reduced LD size (Fig. 3 *E–G*). Conversely, culturing *plxnd1*

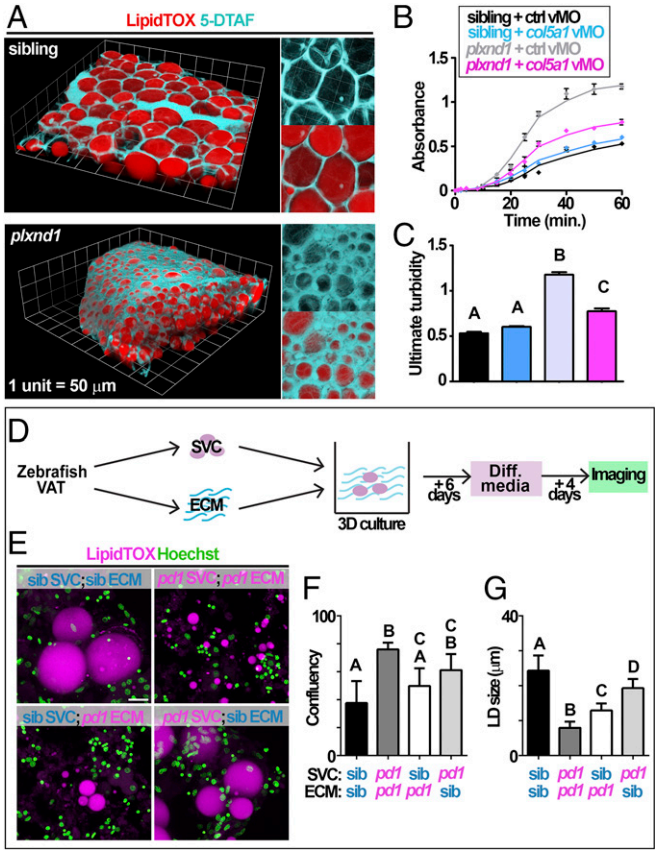

Fig. 3. The extracellular matrix of *plxnd1* mutant VAT is sufficient to induce hyperplastic morphology in a Col5a1-dependent manner. (*A*) 3D renderings of sibling or *plxnd1* mutant VAT stained with LipidTOX (LDs, red) and 5-(4,6-dichlorotriazinyl) aminofluorescein (collagen, cyan). (*B* and *C*) Turbidity assays reveal a Col5a1-dependent increase in the rate of fibrillogenesis (*B*) and a greater ultimate turbidity (*C*), suggesting increased collagen fibrils within *plxnd1* VAT. (*D*) Schematic of ECM and SVC 3D coculture experimental design. Briefly, ECM and SVCs were isolated from either sibling or *plxnd1* mutant VAT. The isolated ECM was then used as a 3D substrate for SVC culture. (*E*) Maximum-intensity projections of adipogenic clusters after 10 d of 3D culture. SVCs were isolated from either sibling (blue) or *plxnd1* (magenta) VAT and used to seed either sibling (blue) or *plxnd1* (magenta) ECM gels. A range in nuclear morphologies was observed in the 3D cultures that likely represents the heterogeneous cellular nature of the stromal vascular fraction. (*F*) Confluency (percentage of field occupied by cells) of 3D cultures. (*G*) Mean LD size of 3D cultures. LD sizes were normally distributed.

mutant SVCs in sibling ECM abrogated the hyperproliferation and smaller LD size observed in the mutant experiment, leading to larger LDs more reminiscent of sibling:sibling cocultures (Fig. 3 *E*–*G*). Moreover, combining ECM extract from siblings and *plxnd1* mutants produced intermediate morphologies dependent on the proportion of wild-type sibling:*plxnd1* mutant ECM (*SI Appendix*, Fig. S13 *B* and *C*), suggesting that the capacity of *plxnd1* mutant ECM to induce proliferation and hyperplastic morphology is proportional to the amount of *plxnd1* mutant ECM present. Injection of *col5a1* vMO before ECM extraction abrogated the ability of *plxnd1* mutant ECM to induce proliferation and hyperplastic morphology in cultured *plxnd1* mutant SVCs (*SI Appendix*, Fig. S13 *D* and *E*). These data demonstrate that *plxnd1* mutant ECM is sufficient to induce hyperproliferation of SVCs and a smaller overall size of LDs.

Lipid Is Preferentially Deposited in SAT of *plxnd1* Mutants Fed a High-Fat Diet. Considering the global obesity epidemic and the influence of body fat distribution on metabolic dysfunction, we next examined the effect of a high-fat diet on regional adiposity and metabolism in *plxnd1* mutant zebrafish. We used daily immersion in 5% chicken egg yolk over the course of 2–3 wk as a high-fat dietary supplement (HFD); this has previously been shown to induce lipid accumulation and metabolism in zebrafish (29–32). HFD treatment led to equivalent increases in lipid accumulation in both *plxnd1*/+ heterozygotes and homozygous *plxnd1* mutants (Fig. 4 *A* and *B* and *SI Appendix*, Fig. S14*A*). A substantial increase in total VAT and SAT area (*SI Appendix*, Fig. S14 *B* and *C*) and VAT and SAT LD size was observed in heterozygotes (Fig. 4 *A*, *D*–*G*). However, VAT in HFD fed *plxnd1* mutants did not expand (*SI Appendix*, Fig. S14*B*), and VAT-LDs did not substantially increase in size (Fig. 4 *A*, *D*–*G*). Strikingly, *plxnd1* mutants underwent a larger expansion of SAT compared with heterozygotes (*SI Appendix*, Fig. S14*C*), leading to supersized SAT-LDs (Fig. 4 *A*, *E*, and *G*) and a decreased VAT:SAT ratio (Fig. 4*C*). Together, these data show that the absence of Plxnd1 results in a preferential expansion of SAT in response to HFD, and thus leads to further exacerbation of altered body fat distribution.

Plxnd1 Deficiency Protects Zebrafish from High-Fat Diet-Induced Insulin Resistance. We hypothesized that decreased VAT:SAT ratio in *plxnd1* mutants was associated with improved insulin sensitivity. HFD-fed wild-type siblings had hyperglycemia (Fig. 5*A*). Further, after a glucose tolerance test, siblings fed a HFD failed to normalize blood glucose levels, suggesting a degree of systemic insulin resistance (Fig. 5*B*). In contrast, *plxnd1*

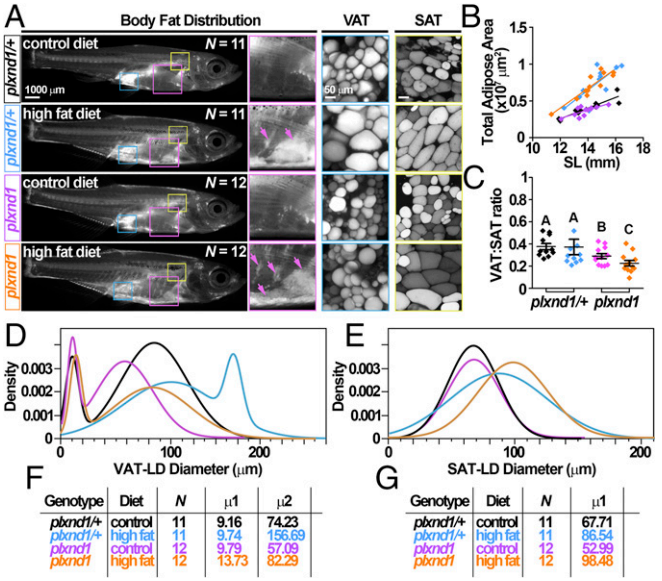

Fig. 4. VAT fails to expand in homozygous *plxnd1* mutants fed a high-fat diet, leading to disproportionately large increases in SAT. (*A*) Nile Red-stained zebrafish after 14 d of normal or high-fat diet. Groups were either *plxnd1* homozygous mutants (*plxnd1*) or *plxnd1* heterozygotes (*plxnd1*/+). (*Left*) Whole-animal body fat distribution, with areas enlarged on the right denoted by colored boxes. Experimental groups are colorized (*plxnd1*/+ fed control diet, black; *plxnd1*/+ fed high-fat diet, blue; *plxnd1* fed control diet, magenta; *plxnd1* fed high-fat diet, orange). Arrows indicate excess lipid deposition in SAT after feeding of HFD. (*B*) Total adipose area relative to standard length revealed greater lipid storage and deposition after HFD intervention. (*C*) *plxnd1* mutants fed a HFD had a greater VAT:SAT ratio indicating disproportionate lipid storage in SAT. (*D*) Probability density functions of VAT LD sizes. All groups exhibited bimodal LD size distributions. (*E*) Probability density functions of SAT LD sizes. All groups exhibited unimodal LD size distributions. (*F*) Means of bimodal VAT-LD size distributions. (*G*) Means of unimodal SAT-LD size distributions.

mutants fed a HFD did not exhibit hyperglycemia (Fig. 5*A*) and efficiently normalized hyperglycemia after a glucose tolerance test (Fig. 5*B*). The *insulin receptor substrates 1* and *2* (*irs1, irs2*) are negatively regulated in insulin resistance (33–35). However, in both control and HFD-fed *plxnd1* VAT, *irs1* and *irs2* mRNAs were increased compared with siblings, supporting augmented insulin signaling in *plxnd1* mutants (Fig. 5*C*). Together, these data indicate that high-fat feeding induces a state reminiscent of insulin resistance in wild-type sibling zebrafish, and Plxnd1 deficiency protects from HFD-induced insulin resistance.

Increased *PLXND1* mRNA in Human VAT Is Associated with Type 2 Diabetes. As Plxnd1 deficiency protects zebrafish from HFD-induced insulin resistance, we hypothesized *PLXND1* mRNA would be positively associated with insulin resistance and type 2 diabetes in humans. Strikingly, analysis of *PLXND1* mRNA levels in VAT and SAT from lean, healthy obese, and type 2 diabetic obese patients revealed that *PLXND1* mRNA was specifically increased in VAT of obese patients with type 2 diabetes (Fig. 5*D*), whereas no change was observed in SAT (Fig. 5*D*) or AT of healthy obese patients (Fig. 5*D*), suggesting a role for VAT *PLXND1* in insulin sensitivity. Moreover, in HFD-fed zebrafish that exhibit features of insulin resistance, VAT-localized *plxnd1* mRNA was up-regulated (*SI Appendix*, Fig. S15*D*), suggesting the positive association between VAT *plxnd1* mRNA levels and insulin resistance is conserved to zebrafish.

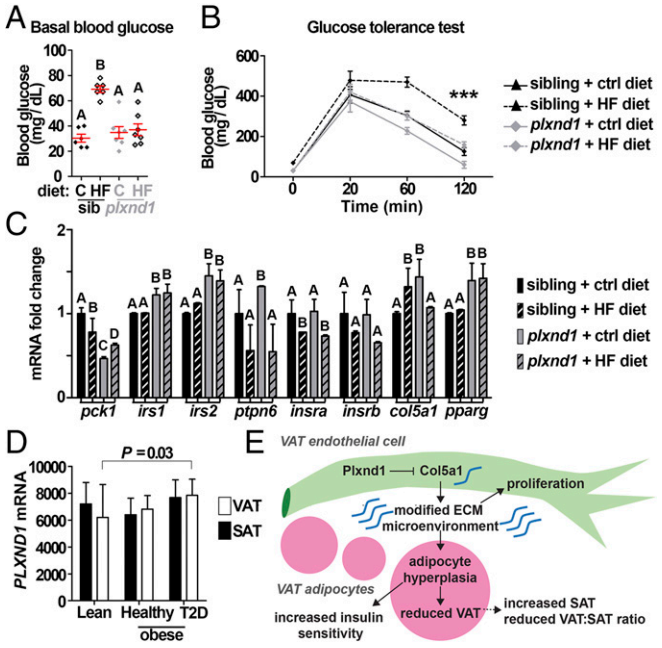

Fig. 5. Mutation of *plxnd1* protects zebrafish from high-fat-diet-induced insulin resistance. (*A*) Basal blood glucose measurements reveal that wild-type siblings fed a high-fat (HF) diet are hyperglycemic. (*B*) Glucose tolerance tests reveal wild-type siblings fed a high-fat (HF) diet have a decreased capacity to normalize blood glucose relative to control-fed siblings ($P < 0.001$). *plxnd1* mutants fed a control diet have an enhanced capacity to normalize blood glucose relative to control-fed siblings ($P < 0.01$), whereas *plxnd1* mutants fed a HF diet have equivalent capacity to normalize experimentally induced hyperglycemia to control-fed siblings ($P > 0.05$). One-factor ANOVA followed by Tukey's HSD test ($\alpha = 0.05$) was used to determine statistical significance at 120 min. (*C*) qRT-PCR analysis of markers of insulin signaling and metabolism in zebrafish VAT. (*D*) *PLXND1* mRNA is significantly up-regulated in VAT, but not SAT, of obese patients with type 2 diabetes. (*E*) Schematic illustrating the current working model of Plxnd1-mediated regulation of VAT morphology.

Discussion

Genome-wide association studies have implicated *PLXND1* in the regulation of body fat distribution and type 2 diabetes (10). However, a role for *PLXND1* in regional adiposity has not been described, nor has direct evidence of a role in human metabolic disease been established. Our data establish three key points. First, Plxnd1 regulates body fat distribution by determining the growth characteristics of VAT. Second, the effect of Plxnd1 in VAT is mediated by Col5a1 and the establishment of an ECM microenvironment that is conducive to hyperplastic growth. Third, Plxnd1 deficiency protects zebrafish from HFD-induced insulin resistance and glucose intolerance, in accord with association data from humans showing that VAT *PLXND1* mRNA levels correlate with insulin resistance and type 2 diabetes. Thus, our data suggest that Plxnd1 promotes VAT hypertrophy and growth and insulin resistance in both zebrafish and humans, and identifies PLXND1 as a new target for treatment of metabolic disease.

We propose a model whereby Plxnd1 regulates the mechanism of VAT growth by determining the status of the VAT ECM microenvironment (Fig. 5*E* and *SI Appendix*, Fig. S16). Our data show that in Plxnd1-deficient VAT, the induction of Col5a1 promotes adipocyte proliferation and differentiation, leading to hyperplastic VAT morphology and reduced lipid accumulation. Moreover, our data show that Col5a1 induction in *plxnd1* mutants is localized to vascular endothelial cells, suggesting that blood vessels are the source of altered VAT morphology and body fat distribution. In normally fed animals, SAT is not significantly affected by Plxnd1 deficiency. However, after high-fat feeding of *plxnd1* mutants, VAT fails to expand, and excess lipid is stored in SAT. Thus, we propose that impaired VAT expansion in *plxnd1* mutants leads to increased, and perhaps compensatory, lipid storage in SAT. A VAT-specific role for Plxnd1 is supported by gene expression data from humans that show *PLXND1* mRNA is positively correlated with hypertrophic morphology in VAT, with no association found between morphology and *PLXND1* in SAT.

The relative abundance of VAT and SAT strongly influence susceptibility to metabolic disease. Previous studies suggest that impaired SAT expansion leads to increased lipid accumulation in VAT and subsequent metabolic complications (36–38). As such, SAT acts as a "lipid buffer" that protects other tissues, including VAT, from excessive lipid exposure. In a similar manner, our HFD data suggest that impaired VAT growth in *plxnd1* mutants positively influences lipid deposition in SAT. Intriguingly, the thiazolidinedione class of peroxisome-proliferator activated receptor ligands influences body fat distribution and decreases VAT:SAT ratio (39–41). Interestingly, we observe an increase in *pparg* mRNA in both control and HFD-fed *plxnd1* VAT, suggesting *pparg* induction within VAT may underlie the observed altered body fat distribution. In accordance, thiazolidinedione treatment has been shown to solely influence VAT growth in humans (40), although other studies suggest SAT is also affected (39). An increased proportion of small adipocytes in SAT is correlated with metabolic disturbance (38, 42). We found *plxnd1* mutants had an increased ratio of small:large LDs in VAT (*SI Appendix*, Fig. S17); however, as we observe increased proliferation and differentiation in *plxnd1* mutant VAT, we believe this phenotype is likely different from the impaired differentiation observed in human insulin-resistant SAT (38).

Type V collagens have not been previously implicated in the regulation of in vivo AT growth or body fat distribution. Type V collagens are expressed by preadipocytes (43) and have a stimulatory effect on adipocyte hyperplasia (19). Indeed, adipocyte differentiation is characterized by increased collagen V accumulation, followed by a decline in collagen V as adipose maturation proceeds (20). Thus, collagen V is associated with "hyperplastic" adipose conditions. Our data support a role for

DEVELOPMENTAL BIOLOGY

Col5a1 in hyperplastic AT morphology. We speculate that Col5a1 may be selectively induced in situations in which hyperplastic growth is needed, such as insulin-resistant AT. Collagen in obese AT correlates with insulin resistance and metabolic disease and is thus often considered pathological (44). Our data suggest that increased Col5a1 is metabolically beneficial. Intriguingly, AT of healthy children contains increased collagen accumulation that is correlated with decreased adipocyte size and body mass index (45), suggesting AT collagen can be beneficial to AT growth and expansion in certain human contexts.

Methods

Human Experiments. All human studies were approved by the local committee on ethics at Karolinska Institutet. Informed consent was obtained from all participants. Detailed methods are included in *SI Appendix*.

Zebrafish and Mouse Experiments. All zebrafish and mouse experiments conformed to the Public Health Service Policy on Humane Care and Use of Laboratory Animals, using protocols approved by the Institutional Animal Care and Use Committee of the University of North Carolina at Chapel Hill, Duke University, and the University of Pennsylvania. Detailed zebrafish methods are included in *SI Appendix*.

Statistics. Statistical analyses were conducted in GraphPad Prism 5.04 (GraphPad Software) or JMP Pro-11.0.0 (SAS Institute). For pairwise analyses, independent Student's *t* test was used to compare means assuming unequal variance: ns = not significant ($P > 0.05$); *$P < 0.05$; **$P < 0.01$; ***$P < 0.001$. One-way ANOVA followed by Tukey's HSD test was used when comparing three or more means. Groups with the same letters are not significantly different ($\alpha = 0.05$). Probability density functions were used to describe the likelihood of LD sizes. Bars are mean ± SEM unless stated.

ACKNOWLEDGMENTS. We thank Simon Hughes, Vicki Bautch, Suk-Won Jin, and Florian Ulrich for discussions and comments on the manuscript. We are grateful to Suk-Won Jin for transgenic lines, Jan Rombout for antibodies, the University of North Carolina (UNC) Olympus Research Imaging Center and the Duke University Light Microscopy Core Facility for the use of microscopes, and the Center for Gastrointestinal Biology and Disease Histology Core (P30 DK34987). This work was supported by grants from the NIH (DK081426, DK091356, DK093399 to J.F.R.; HL092263 to J.T.-V.; and R01HL118768 to J.A.E.); from the Swedish Research Council, Swedish Diabetes Association, Novo Nordisk Foundation, Swedish Heart and Lung Foundation, and Strategic Research Programme in Diabetes at Karolinska Institutet (P.A.); a Pilot Research Project Award from the UNC University Cancer Research Fund (J.F.R.); a Pew Scholars in the Biomedical Sciences Award (to J.F.R.); and American Heart Association Postdoctoral Fellowships (11POST7360004 and 13POST16930097 to J.E.N.M.).

1. Salans LB, Knittle JL, Hirsch J (1968) The role of adipose cell size and adipose tissue insulin sensitivity in the carbohydrate intolerance of human obesity. *J Clin Invest* 47(1):153–165.
2. Ahima RS, Lazar MA (2013) Physiology. The health risk of obesity—better metrics imperative. *Science* 341(6148):856–858.
3. Arner E, Arner P (2013) Health and obesity: Not just skin deep. *Science* 342(6158): 558–559.
4. Hoffstedt J, et al. (2010) Regional impact of adipose tissue morphology on the metabolic profile in morbid obesity. *Diabetologia* 53(12):2496–2503.
5. Fox CS, et al. (2007) Abdominal visceral and subcutaneous adipose tissue compartments: Association with metabolic risk factors in the Framingham Heart Study. *Circulation* 116(1):39–48.
6. Snijder MB, van Dam RM, Visser M, Seidell JC (2006) What aspects of body fat are particularly hazardous and how do we measure them? *Int J Epidemiol* 35(1):83–92.
7. Kim JY, et al. (2007) Obesity-associated improvements in metabolic profile through expansion of adipose tissue. *J Clin Invest* 117(9):2621–2637.
8. Sun K, Kusminski CM, Scherer PE (2011) Adipose tissue remodeling and obesity. *J Clin Invest* 121(6):2094–2101.
9. Kusminski CM, et al. (2012) MitoNEET-driven alterations in adipocyte mitochondrial activity reveal a crucial adaptive process that preserves insulin sensitivity in obesity. *Nat Med* 18(10):1539–1549.
10. Shungin D, et al.; ADIPOGen Consortium; CARDIOGRAMplusC4D Consortium; CKDGen Consortium; GEFOS Consortium; GENIE Consortium; GLGC; ICBP; International Endogene Consortium; LifeLines Cohort Study; MAGIC Investigators; MuTHER Consortium; PAGE Consortium; ReproGen Consortium (2015) New genetic loci link adipose and insulin biology to body fat distribution. *Nature* 518(7538):187–196.
11. Gay CM, Zygmunt T, Torres-Vázquez J (2011) Diverse functions for the semaphorin receptor PlexinD1 in development and disease. *Dev Biol* 349(1):1–19.
12. Gitler AD, Lu MM, Epstein JA (2004) PlexinD1 and semaphorin signaling are required in endothelial cells for cardiovascular development. *Dev Cell* 7(1):107–116.
13. Torres-Vázquez J, et al.; Van N Pham (2004) Semaphorin-plexin signaling guides patterning of the developing vasculature. *Dev Cell* 7(1):117–123.
14. Sakurai A, et al. (2010) Semaphorin 3E initiates antiangiogenic signaling through plexin D1 by regulating Arf6 and R-Ras. *Mol Cell Biol* 30(12):3086–3098.
15. Mariman EC, Wang P (2010) Adipocyte extracellular matrix composition, dynamics and role in obesity. *Cell Mol Life Sci* 67(8):1277–1292.
16. Wenstrup RJ, et al. (2011) Regulation of collagen fibril nucleation and initial fibril assembly involves coordinate interactions with collagens V and XI in developing tendon. *J Biol Chem* 286(23):20455–20465.
17. Sun M, et al. (2011) Collagen V is a dominant regulator of collagen fibrillogenesis: Dysfunctional regulation of structure and function in a corneal-stroma-specific Col5a1-null mouse model. *J Cell Sci* 124(Pt 23):4096–4105.
18. Spencer M, et al. (2011) Adipose tissue extracellular matrix and vascular abnormalities in obesity and insulin resistance. *J Clin Endocrinol Metab* 96(12):E1990–E1998.
19. Nakajima I, Muroya S, Tanabe R, Chikuni K (2002) Positive effect of collagen V and VI on triglyceride accumulation during differentiation in cultures of bovine intramuscular adipocytes. *Differentiation* 70(2-3):84–91.
20. Nakajima I, Muroya S, Tanabe R, Chikuni K (2002) Extracellular matrix development during differentiation into adipocytes with a unique increase in type V and VI collagen. *Biol Cell* 94(3):197–203.
21. Flynn EJ, 3rd, Trent CM, Rawls JF (2009) Ontogeny and nutritional control of adipogenesis in zebrafish (Danio rerio). *J Lipid Res* 50(8):1641–1652.
22. Minchin JE, Rawls JF (2011) In vivo analysis of white adipose tissue in zebrafish. *Methods Cell Biol* 105:63–86.
23. Song Y, Cone RD (2007) Creation of a genetic model of obesity in a teleost. *FASEB J* 21(9):2042–2049.
24. Tingaud-Sequeira A, Ouadah N, Babin PJ (2011) Zebrafish obesogenic test: A tool for screening molecules that target adiposity. *J Lipid Res* 52(9):1765–1772.
25. McMenamin SK, Minchin JE, Gordon TN, Rawls JF, Parichy DM (2013) Dwarfism and increased adiposity in the gh1 mutant zebrafish vizzini. *Endocrinology* 154(4): 1476–1487.
26. Imrie D, Sadler KC (2010) White adipose tissue development in zebrafish is regulated by both developmental time and fish size. *Dev Dyn* 239(11):3013–3023.
27. Sakurai A, et al. (2011) Phosphatidylinositol-4-phosphate 5-kinase and GEP100/Brag2 protein mediate antiangiogenic signaling by semaphorin 3E-plexin-D1 through Arf6 protein. *J Biol Chem* 286(39):34335–34345.
28. Lackey DE, et al. (2014) Contributions of adipose tissue architectural and tensile properties toward defining healthy and unhealthy obesity. *Am J Physiol Endocrinol Metab* 306(3):E233–E246.
29. Semova I, et al. (2012) Microbiota regulate intestinal absorption and metabolism of fatty acids in the zebrafish. *Cell Host Microbe* 12(3):277–288.
30. Walters JW, Anderson JL, Bittman R, Pack M, Farber SA (2012) Visualization of lipid metabolism in the zebrafish intestine reveals a relationship between NPC1L1-mediated cholesterol uptake and dietary fatty acid. *Chem Biol* 19(7):913–925.
31. Carten JD, Bradford MK, Farber SA (2011) Visualizing digestive organ morphology and function using differential fatty acid metabolism in live zebrafish. *Dev Biol* 360(2):276–285.
32. Marza E, et al. (2005) Developmental expression and nutritional regulation of a zebrafish gene homologous to mammalian microsomal triglyceride transfer protein large subunit. *Dev Dyn* 232(2):506–518.
33. Capiotti KM, et al. (2014) Persistent impaired glucose metabolism in a zebrafish hyperglycemia model. *Comp Biochem Physiol B Biochem Mol Biol* 171:58–65.
34. Goodyear LJ, et al. (1995) Insulin receptor phosphorylation, insulin receptor substrate-1 phosphorylation, and phosphatidylinositol 3-kinase activity are decreased in intact skeletal muscle strips from obese subjects. *J Clin Invest* 95(5):2195–2204.
35. Ruiz-Alcaraz AJ, et al. (2005) A novel regulation of IRS1 (insulin receptor substrate-1) expression following short term insulin administration. *Biochem J* 392(Pt 2):345–352.
36. Virtue S, Vidal-Puig A (2010) Adipose tissue expandability, lipotoxicity and the Metabolic Syndrome—an allostatic perspective. *Biochim Biophys Acta* 1801(3):338–349.
37. McLaughlin T, Lamendola C, Liu A, Abbasi F (2011) Preferential fat deposition in subcutaneous versus visceral depots is associated with insulin sensitivity. *J Clin Endocrinol Metab* 96(11):E1756–E1760.
38. McLaughlin T, et al. (2007) Enhanced proportion of small adipose cells in insulin-resistant vs insulin-sensitive obese individuals implicates impaired adipogenesis. *Diabetologia* 50(8):1707–1715.
39. McLaughlin TM, et al. (2010) Pioglitazone increases the proportion of small cells in human abdominal subcutaneous adipose tissue. *Obesity (Silver Spring)* 18(5):926–931.
40. Kelly IE, Han TS, Walsh K, Lean ME (1999) Effects of a thiazolidinedione compound on body fat and fat distribution of patients with type 2 diabetes. *Diabetes Care* 22(2): 288–293.
41. Hwang YC, et al. (2008) Effects of rosiglitazone on body fat distribution and insulin sensitivity in Korean type 2 diabetes mellitus patients. *Metabolism* 57(4):479–487.
42. McLaughlin T, et al. (2014) Subcutaneous adipose cell size and distribution: Relationship to insulin resistance and body fat. *Obesity (Silver Spring)* 22(3):673–680.
43. Hocking SL, Wu LE, Guilhaus M, Chisholm DJ, James DE (2010) Intrinsic depot-specific differences in the secretome of adipose tissue, preadipocytes, and adipose tissue-derived microvascular endothelial cells. *Diabetes* 59(12):3008–3016.
44. Sun K, Tordjman J, Clément K, Scherer PE (2013) Fibrosis and adipose tissue dysfunction. *Cell Metab* 18(4):470–477.
45. Tam CS, Tordjman J, Divoux A, Baur LA, Clément K (2012) Adipose tissue remodeling in children: The link between collagen deposition and age-related adipocyte growth. *J Clin Endocrinol Metab* 97(4):1320–1327.